

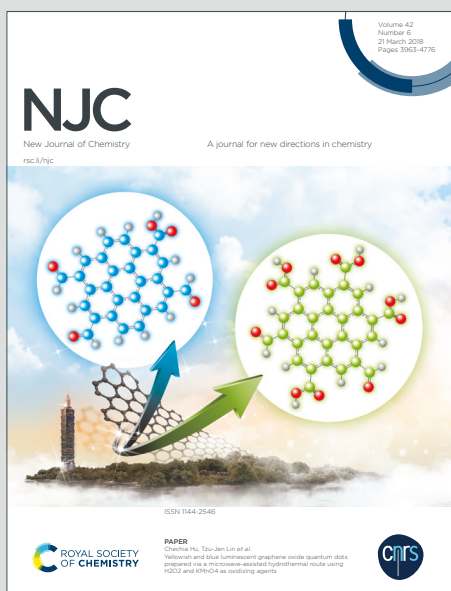
NJC

New Journal of Chemistry

Accepted Manuscript

A journal for new directions in chemistry

This article can be cited before page numbers have been issued, to do this please use: J. Guo, G. Zhang, Z. Tang and J. Zhang, *New J. Chem.*, 2020, DOI: 10.1039/D0NJ04419A.



This is an Accepted Manuscript, which has been through the Royal Society of Chemistry peer review process and has been accepted for publication.

Accepted Manuscripts are published online shortly after acceptance, before technical editing, formatting and proof reading. Using this free service, authors can make their results available to the community, in citable form, before we publish the edited article. We will replace this Accepted Manuscript with the edited and formatted Advance Article as soon as it is available.

You can find more information about Accepted Manuscripts in the [Information for Authors](#).

Please note that technical editing may introduce minor changes to the text and/or graphics, which may alter content. The journal's standard [Terms & Conditions](#) and the [Ethical guidelines](#) still apply. In no event shall the Royal Society of Chemistry be held responsible for any errors or omissions in this Accepted Manuscript or any consequences arising from the use of any information it contains.

1
2
3
4
5
6
7
8
9
10
11
12
13
14
15
16
17
18
19
20
21
22
23
24
25
26
27
28
29
30
31
32
33
34
35
36
37
38
39
40
41
42
43
44
45
46
47
48
49
50
51
52
53
54
55
56
57
58
59
60

Design of Prussian blue analogues derives double-cone structure Ce-Fe catalysts and their enhanced performances for the selective catalytic reduction of NO_x with NH₃

Jie Guo^{a,b}, Guodong Zhang^a, Zhicheng Tang^{a,c*}, Jiyi Zhang^{b*}

(a. State Key Laboratory for Oxo Synthesis and Selective Oxidation, National Engineering

Research Center for Fine Petrochemical Intermediates, Lanzhou Institute of Chemical Physics,

Chinese Academy of Sciences, Lanzhou 730000, PR China

b. School of petroleum and chemical, Lanzhou University of Technology, Lanzhou 730050,

China.

c. Dalian National Laboratory for Clean Energy, Dalian Institute of Chemical Physics, Chinese

Academy of Sciences, Dalian, 116023, China)

*Corresponding author. Tel.: +86-931-4968083, Fax: +86-931-4968019, E-mail address:

tangzhicheng@licp.cas.cn (Z.Tang); zhangjiyi@lut.cn (J.Zhang).

Abstract

Prussian blue (PB) and its analogues (PBA) with differences in structure and adjustable composition have been recognized as promising materials for catalysis, energy storage, and biological applications. Here, a simple surface anchoring strategy is proposed to achieve the uniform deposition of CeO₂ nanocrystals on the double-cone structure PBA surface (denoted Ce@Ce-Fe catalyst) for the selective catalytic reduction of NO_x with NH₃ (NH₃-SCR). Compared with Ce-Fe and Ce@CeO₂-Fe₂O₃, Ce@Ce-Fe catalyst exhibited enhanced catalytic activity, more

extensive working temperature window, improved SO₂ tolerance, implying their good application in the process of NH₃-SCR. Moreover, the catalysts have been characterized systematically to elucidate their surface properties and morphological structure. Taking advantages of the excellent redox performance, unique morphology, mesoporous structure with big surface area and pore diameter, and more acid amount, the Ce@Ce-Fe catalyst exhibits higher deNO_x performance. In addition, the Ce@Ce-Fe catalyst also manifests significant resistance of H₂O and SO₂ due to the higher content of Fe atom ratio, implying that Fe acted a critical role in Ce-Fe based catalytic system. More importantly, the present study indicates that well-dispersed active components and unique architectures can effectively enhance the performance of catalysts.

Key words: NH₃-SCR; Prussian blue analogues; Ceria anchoring; double-cone structure; resistance of H₂O and SO₂

1. Introduction

Under the premise of the rapid development of urbanization and industrialization, the proportion of air pollution in environmental pollution has gradually increased [1-5]. Nitrogen oxides (NO_x) is regarded as a common air pollutants, which is the main cause of photochemical smog, destruction of the ozone layer, and acid rain [6, 7]. Currently, the SCR technology has been proven to be a very mature technology with great promise for the removal of nitrogen oxides and has been successfully applied to industrial application. Furthermore, vanadium-based catalyst has been developed an

1
2
3
4 industrialized and commercial catalysts due to its high catalytic activity and
5
6 selectivity. Unfortunately, the drawbacks of V-based catalysts still existed, such as
7
8 poor thermal stability, narrow operating temperature window and toxicity of
9
10 vanadium species [8, 9]. Therefore, further seeking of high-performance,
11
12 cost-efficient and environment friendly catalysts with abundant resources for
13
14 replacement of previous catalysts for NH₃-SCR were urgently needed.
15
16
17
18
19
20

21
22 Ce-based catalysts among rare earth-based catalysts had non-toxicity, excellent
23
24 oxygen storage capacity and redox characteristics, which were considered as good
25
26 substitutes for V-based catalysts [10-12]. In the NH₃-SCR catalytic reaction process, a
27
28 catalytic cycle could be completed when Ce⁴⁺ and Ce³⁺ were converted to each other
29
30 in the catalytic system. In the above process, the Ce³⁺ substance was essential to
31
32 increase the catalytic activity of the NH₃-SCR reaction, and the formed oxygen
33
34 vacancies also promoted the NH₃-SCR reaction [13]. However, Ce-based catalysts
35
36 were easily poisoned by SO₂ in flue gas while Ce and SO₂ undergo oxidation
37
38 reactions to produce Ce₂(SO₄)₃, thereby destroying the mutual conversion of Ce⁴⁺ and
39
40 Ce³⁺ species [14]. Therefore, the modification research based on Ce-based catalysts
41
42 has been widely studied for NH₃-SCR in recent years [15-19]. Interestingly, Fe-based
43
44 catalyst was a typical active ingredient or promoter in NH₃-SCR system, which
45
46 exhibited good NH₃-SCR activity, N₂ selectivity and non-poison due to its inherently
47
48 environmentally friendly character, prominent thermal stability and outstanding
49
50 resistance of H₂O/SO₂ [20-22]. Based on above conclusions, Fe-based catalyst could
51
52 be a suitable candidate and promoter to improve the resistance of H₂O/SO₂.
53
54
55
56
57
58
59
60

Therefore, further exploitation of Ce-Fe types of NH_3 -SCR catalyst is of special interest.

Prussian blue analogue (PBA) is a type of crystalline metal organic framework (MOF) composed of divalent and trivalent metal ions bridged by cyanide ligands [23, 24]. It could be made into compounds with uniform composition and size as well as various forms and structures [25, 26]. Due to its special thermal properties and unique reactivity, PBA could be used as a precursor for the synthesis of layered materials with hollow or porous structures [27, 28]. Recently, PBA was able to create special and enhanced structural and physicochemical properties. Furthermore, this materials have great potential serving as building components for catalysts. More interestingly, PBA also owed unique morphology and structure by adjusting methods of synthesis, making it ideal precursors for fabrication of novel catalysts for NH_3 -SCR reaction.

In our work, we report the fabrication of Prussian blue analogues of Ce-Fe catalysts derived from the potassium ferricyanide as the precursor framework and cerium as the metal salt solution which was synthesized using a simple co-precipitation method. In addition, the optimal catalyst was determined by changing the synthesis conditions. On this basis, in order to further improve catalytic activity, Ce@Ce-Fe and Ce@CeO₂-Fe₂O₃ catalysts were synthesized by anchoring Ce on surface of Ce-Fe precursors and CeO₂-Fe₂O₃ oxide, respectively. Moreover, the resulting Ce@Ce-Fe catalyst with unique morphology and structure exhibited a better operating temperature window, excellent catalytic activity than other catalysts. Hence,

it was critical to investigate the structure and morphology of the catalyst and the effect of Ce anchoring on the surface of catalyst.

2 Experimental

2.1 Preparation of samples

The specific synthesis steps were as follows:

(1) Synthesis of Ce-Fe Prussian blue precursor

0.17 g of cerium acetate ($\text{Ce}(\text{CH}_3\text{COO})_3$) and 1.2 g of polyvinylpyrrolidone (PVP, K-30) were dissolved in a mixed solution of 20 ml of ethanol and 10 ml of deionized water, referred to as solution A; 0.192 g of potassium ferricyanide ($\text{K}_3[\text{Fe}(\text{CN})_6]_2$) was dissolved in 25 ml of deionized water solution and recorded it as solution B; solution B was added dropwise to solution A, stirred evenly under the same temperature, and aged for 24 h at room temperature. Next, the suspension was centrifuged, and the obtained product was washed with ethanol and deionized water alternately at least five times, dried at 60 °C for 12 h, and the obtained product was recorded as Ce-Fe catalyst.

Repeated the above experiment, only changed the amount of PVP to 0.6 g, the concentration of metal salt solution was reduced by half and the molar ratio of Ce and Fe became 1: 1, and the products obtained were respectively denoted Ce-Fe-PVP, Ce-Fe-C and Ce-Fe-M catalyst.

(2) Synthesis of $\text{CeO}_2\text{-Fe}_2\text{O}_3$ Prussian blue catalyst

The above-prepared Ce-Fe-based Prussian blue precursor was calcined at 400 °C for 5 h at a temperature increase rate of 1 °C/min, and, and the obtained products were

denoted CeO₂-Fe₂O₃ catalyst.

View Article Online
DOI: 10.1039/D0NJ04419A

(3) Synthesis of Ce@Ce-Fe catalyst

0.1 g Ce-Fe Prussian blue precursor was ultrasonically dispersed in a mixed solution of 40 ml water and 40 ml absolute ethanol, and then 0.2 g of hexamethylenetetramine (C₆H₁₂N₄) and 0.15 g cerium acetate hexahydrate (Ce(NO₃)₃·6H₂O) were added sequentially with magnetic stirring. The suspension was further heated to 70 °C and maintained for 2 h. After natural cooling to room temperature, the product was collected by centrifugation and washed twice with deionized water, then dried at 60 °C for 12 h, calcined at 400 °C for 3 h at a heating rate of 1 °C/min, and the obtained product was Ce@Ce-Fe catalyst.

(4) Synthetic Ce@CeO₂-Fe₂O₃ catalyst

Repeat (3) the experimental procedure, only 0.1 g Ce-Fe precursor is replaced with 0.1 g CeO₂-Fe₂O₃ oxides, and the resulting product was recorded as Ce@CeO₂-Fe₂O₃ catalyst.

2.2 Characterizations of catalysts

The morphology of samples was illustrated by using a scanning electron microscope (SEM). In addition, the SEM image was recorded on the JSM-6701F emission scanning electron microscope, and the profiles of SEM were recorded at 30 kV.

Transmission electron microscopy (TEM) experiments of catalysts were carried out on a JEOL JEM-2010 transmission electron microscope with an operating voltage of 200 kV.

1
2
3
4 Brunauer-Emmett-Teller (BET) surface area, pore size and pore volume of
5
6 sample was carried out by nitrogen adsorption and desorption at 76.2 K on the
7
8 Micromeritics ASAP 2020 instrument.
9
10

11
12 Powder X-ray diffraction (XRD) patterns analysis of catalysts were exhibited
13
14 by a D8 discover X-ray diffractometer, which varied from 10° to 90° with a scanning
15
16 speed of 0.5° min⁻¹.
17
18

19
20 Raman Spectroscopy (RS) was conducted by a confocal Raman spectrometer
21
22 (Horiba JobinYvon S. A. S, France) with an argon green ion laser (532 nm).
23
24

25
26 X-ray photoelectron spectroscopy (XPS) data was collected on a VG
27
28 ESCALAB 210 Electron Spectrometer (Mg Ka radiation; $h\nu = 1253.6$ eV), and XPS
29
30 data was calibrated as the standard by using the C 1s binding energy of 284.6 eV.
31
32

33
34 Temperature program reduction with hydrogen (H₂-TPR) was carried out by
35
36 DAS-7000 automatic multi-function adsorption apparatus. In general, 50 mg catalyst
37
38 sample was performed on the quartz tube reactor, and the temperature ranged from
39
40 room temperature to 850 °C with a heating rate of 10 °C min⁻¹. Furthermore, 5 vol.%
41
42 H₂ balanced N₂ was used with a flow rate of 40 mL min⁻¹.
43
44

45
46 Temperature program desorption of NH₃ (NH₃-TPD) was carried out by
47
48 DAS-7000 automatic multi-function adsorption apparatus. Before each analysis, the
49
50 catalyst sample was purged at 300 °C with a He gas for 30 min. Furthermore, 50 mg
51
52 sample of catalyst was performed on the quartz tube reactor, and the temperature
53
54 varied from 100 °C to 650 °C with a heating rate of 10 °C min⁻¹. Moreover, 5 vol. %
55
56 NH₃ balanced He was used with a flow rate of 40 mL min⁻¹.
57
58
59
60

Fourier Transform Infrared Spectroscopy (FTIR) was scanned with a resolution of 4 cm⁻¹ by Nexus 870 under a range of 400-4000 cm⁻¹ at room temperature.

2.3 NH₃-SCR activity measurements

The detailed measurement process is shown in the supplementary information.

3 Result and discussion

3.1 Morphology of sample

The scanning electron microscope (SEM) of the Ce-Fe-PVP, Ce-Fe-M, Ce-Fe and Ce@Ce-Fe precursors is presented in Fig. 1. As could be observed from Fig. 1a, b, Ce-Fe-PVP had a uniform double-cone dodecahedron structure with the same particle size, and at the same time, the size of each face of the double-cone dodecahedron was also basically the same. However, the particle size of the Ce-Fe-PVP catalyst precursor was relatively large. According to reports in related literature, the amount of PVP could control the size of the particle size, and the particle size was too large would affect the catalytic activity of the catalyst. According to Fig. 1c, d, the precursor of Ce-Fe-M catalyst also has a double-cone structure, and the particle size was relatively uniform. Although the twelve faces on the precursor were not very obvious, they could also be observed to faceted structure. The particle size of the catalyst precursor of Ce-Fe-M was small, which was beneficial to the improvement of the NO conversion in the catalytic reaction, but the molar ratio between Ce and Fe might affect the catalytic activity of the catalyst, which would be described during the characterization work. Specially, the Ce-Fe catalyst is shown in Fig. 1e, f. The morphology of the catalyst precursor in the figure was also a

double-cone structure, the size and structure were uniform, and the particle size was basically the same. In summary, the precursors of Ce-Fe catalysts all exhibited a double-cone structure, the PVP and molar ratio would affect the structure size of the catalyst, and indirectly affect the activity of the catalyst. Meanwhile, Ce@Ce-Fe catalyst is presented in Fig. 1g, h. It was clear that the morphology of precursor was also a double-cone structure, the size and structure were uniform, and the particle size was basically the same. According to these study, exploring the size of the catalytic structure and the effect of morphology on the catalytic performance of the catalyst.

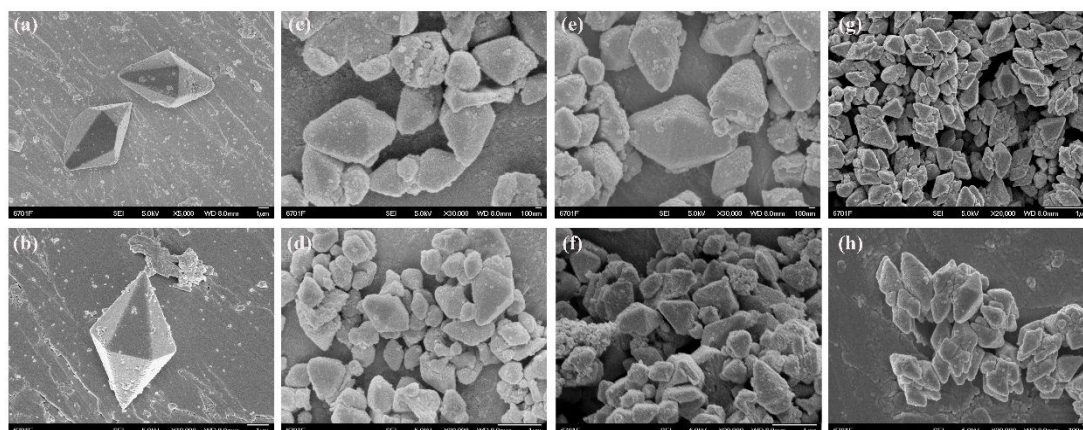


Fig. 1 SEM micrographs of precursors: Ce-Fe-P (a, b), Ce-Fe-M (c, d), Ce-Fe (e, f) and Ce@Ce-Fe (g, h).

Fig. 2 presents a typical low-magnification transmission electron microscopy (TEM) image of the three samples, which further formed the unique morphology of the catalyst. The morphology was consistent with the SEM images. The selected-area electron-diffraction pattern (SAED) in Fig. 2c, there was three diffraction rings indicating that the Ce@Ce-Fe was pleomorphic. The elemental analysis exerted a significant role in the exploration of distribution of iron and cerium. Furthermore,

1
2
3
4 from the high-resolution transmission electron microscope image (HRTEM) in Fig. 2b,
5
6 it can be clearly seen that the well-defined pores with a uniform diameter in
7
8 Ce@Ce-Fe, which further confirmed the mesoporous feature of the Ce@Ce-Fe. The
9
10 result of mapping spectra of the Ce@Ce-Fe was tested in Fig. 2i-g. It was proved that
11
12 Ce@Ce-Fe was consisted of Ce and Fe element, and Fig. 2i-g also shows the
13
14 existence of Ce and Fe, which were uniformly distributed. Meanwhile, according to
15
16 Fig. S1, the element atomic of Ce was 67.95% while the element atomic of Fe was
17
18 32.05%. Notably, the presence of Ce was more spersed, indicating that the
19
20 successfully anchoring of Ce on the surface of Ce-Fe precursor, which could enhance
21
22 the catalytic performance, because the atomic of Ce has excellent redox. In addition,
23
24 the introduction of Ce and Fe increased the redox of materials and the tolerance of
25
26 SO₂.

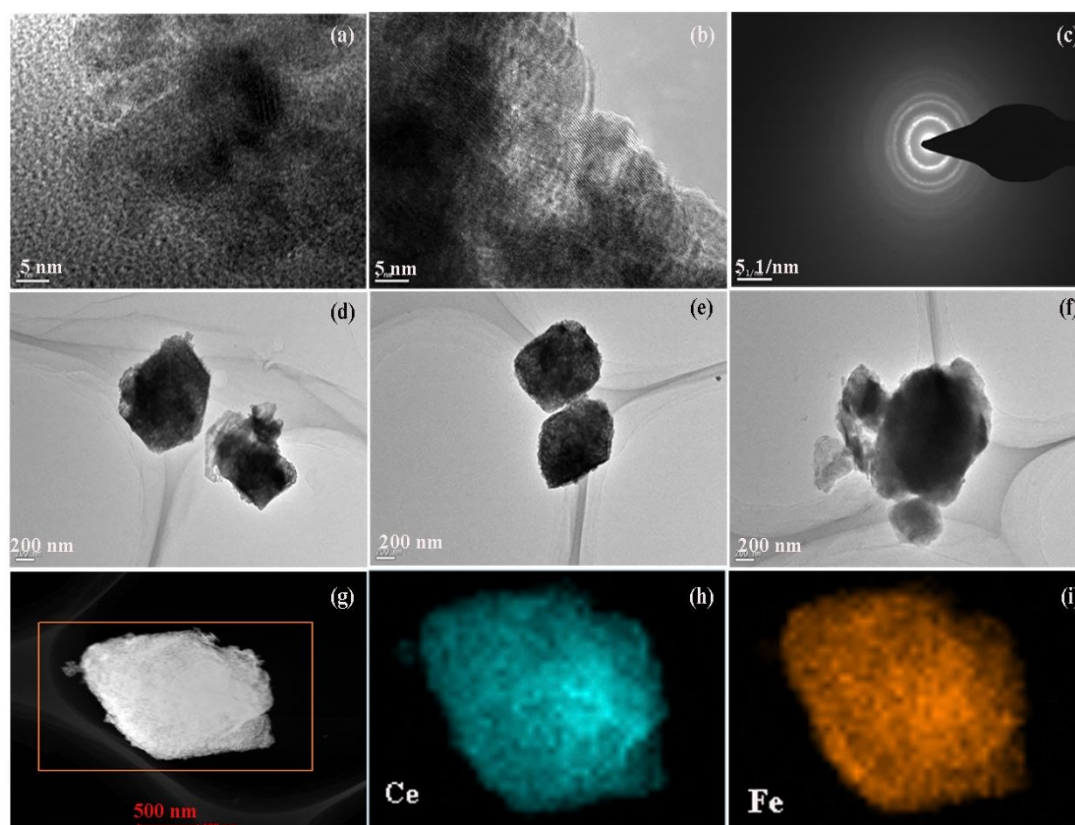


Fig. 2 TEM images of Ce-Fe (a, d), Ce@Ce-Fe (b, c, e) and mapping (g, h, i),

Ce@CeO₂-Fe₂O₃ (f).

3.2 Structure of sample

As shown in Fig. 3a, the typical diffraction peaks of fluorite cubic structure could be observed in the three types of Prussian blue synthetic materials Ce-Fe, Ce@Ce-Fe and Ce@CeO₂-Fe₂O₃. It could be observed that the diffraction peaks at 28.5°, 33.0°, 47.5°, 56.4°, 69.4°, and 76.9° could be attributed to (111), (200), (220), (222), (400), and (420) planes of CeO₂, respectively (PDF#78-0694, Fm3m). And it was clearly observed that the diffraction peaks of ferric oxide were not detected in the materials of Ce-Fe, Ce@Ce-Fe and Ce@CeO₂-Fe₂O₃ catalysts, which indicated that ferric oxide of these three catalysts were evenly dispersed on the catalyst. In addition, it was worth noting that the peak intensity of the Ce@Ce-Fe catalyst was the strongest, indicating that the crystallinity of the catalyst was higher.

Fig. 3b presents the Raman spectra of Ce-Fe, Ce@Ce-Fe and Ce@CeO₂-Fe₂O₃ catalyst. For mixed oxides, the main energy band was also observed around 460 cm⁻¹, and as Ce anchors from Ce-Fe precursors to Ce-Fe oxides, the energy band sequentially shifted to lower frequencies [29]. In the Raman spectrum of fluorite-type oxides, it had been reported that the red shifted of the ceria band was related to lattice shrinkage due to cation doping [30]. It should be emphasized that through XRD measurement, the lattice shrinkage of CeO₂ after Ce anchoring was very limited, but the Raman shift of the cerium oxide band was obvious. This phenomenon indicated that the content of Ce-Fe catalyst was inconsistent, and the content of Ce anchoring

on the surface of the solid solution was higher than the content of Ce in the catalyst [31]. The high Ce content caused the full width at half maximum (FWHM) of the main band of ceria to widen, indicating that the crystallite size of ceria was small, which was beneficial to enhance the catalytic performance. [32]. According to the findings of XRD and Raman, it was clear that after Ce was anchored, it would have a significant effect on the structure of Ce-Fe catalyst.

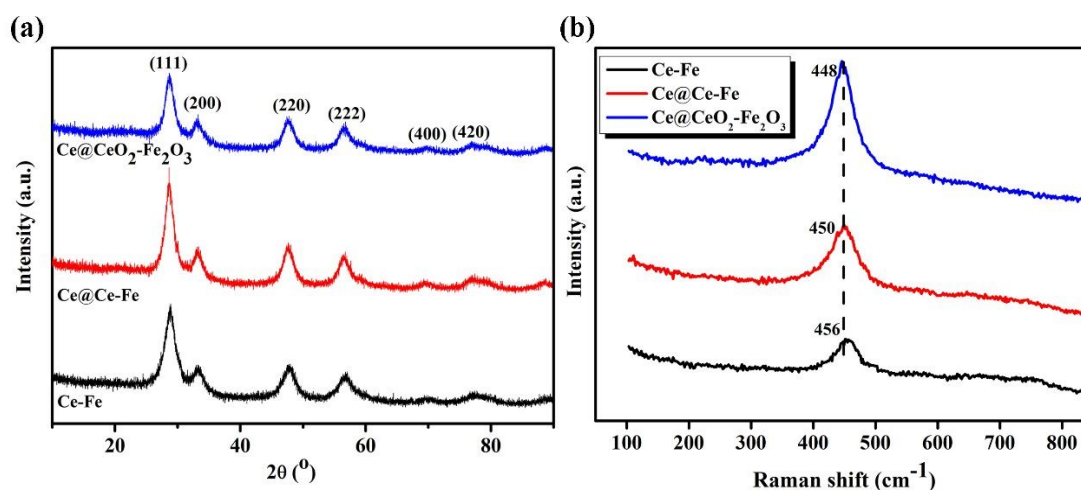


Fig. 3 XRD spectrum of catalysts (a); Raman spectrum of catalysts (b).

The specific surface area, pore size and pore volume of the three catalysts and precursors are shown in Table 1. According to Table 1, the BET specific surface areas of Ce-Fe-P, Ce@Ce-Fe-P and Ce@CeO₂-Fe₂O₃-P precursors were 61.1, 44.6 and 89.2 m²g⁻¹, respectively. Meanwhile, the pore diameters of Ce-Fe-P, Ce@Ce-Fe-P and Ce@CeO₂-Fe₂O₃-P precursors are 14.0, 16.7 and 10.7 nm, respectively; the pore volumes of different precursors are 0.2, 0.2 and 0.2 m³g⁻¹, respectively. In the alkaline environment, the Ce anchored the precursor, the pores were blocked or Ce was

1
2
3
4 successfully anchored above the surface of the precursors, so that the BET specific
5
6 surface areas of the Ce anchor precursor was reduced; but for the Ce anchors the
7
8 oxide, it was happened to erosion, increasing the BET specific surface areas of the Ce
9
10 anchored oxide. Meanwhile, the BET specific surface areas of Ce-Fe, Ce@Ce-Fe and
11
12 Ce@CeO₂-Fe₂O₃ catalysts were 40.3, 26.6 and 81.2 m²g⁻¹, respectively. Moreover,
13
14 the pore diameters of Ce-Fe, Ce@Ce-Fe and Ce@CeO₂-Fe₂O₃ catalysts were 5.9, 6.9
15
16 and 10.5 nm, respectively; the pore volumes of different precursors were 0.1, 0.1 and
17
18 0.2 m²g⁻¹, respectively. Compared with the precursor, the BET specific surface area of
19
20 the catalyst was reduced. Because during calcination, the internal pores would sinter
21
22 and collapse, resulting in a decrease in the specific surface area of the catalyst. The
23
24 nitrogen adsorption and desorption curves of precursors and catalysts are shown in
25
26 Fig. 4a, b. In addition, in the Brunauer classification, the N₂ adsorption and desorption
27
28 curves of these three catalysts corresponded to type IV isotherms in Fig. 4b.
29
30 According to the IUPAC classification, the hysteresis loop of the three catalysts was
31
32 H₃ type, indicating that all three catalysts exhibited a typical mesoporous structure.
33
34 After Ce anchored the Ce-Fe precursor, the BET surface area of the Ce@Ce-Fe-P
35
36 precursor and Ce@Ce-Fe catalyst were both reduced to some extent. This was because
37
38 the anchored Ce could partially cover the accumulation pores. Therefore, after Ce was
39
40 anchored, the average pore size of Ce@Ce-Fe-P precursor and Ce@Ce-Fe catalyst
41
42 decreased, which was similar to previous reports. In addition, Fig. 5 also shows the
43
44 pore size distribution curve of the BJH about precursors and catalysts. It was worth
45
46 noting that the pore sizes of the three catalysts were mainly distributed between 2 and
47
48
49
50
51
52
53
54
55
56
57
58
59
60

50 nm, which mean that hree catalysts all exhibited typical mesoporous structures, which was consistent with the results in Fig. 4. At the same time, the nitrogen adsorption and desorption curves, and BJH pore size distribution curves of three catalysts showed typical mesoporous structures. Based on the above conclusions, it could be concluded that the Ce-Fe-based Prussian blue catalyst had a typical mesoporous structure, which was beneficial to the dispersion of active ingredients, exposure of more active sites and adsorption of reactants. In general, these factors were critical to improve the catalytic performance of the catalyst.

Table 1 Surface area, pore characteristics of different catalysts and precursors.

Sample	Surface area (m ² g ⁻¹)	Pore size (nm)	Pore volume (m ³ g ⁻¹)	Crystal size (nm)
Ce-Fe-P	61.1	14.0	0.2	-
Ce@Ce-Fe-P	44.6	16.7	0.2	-
Ce@CeO ₂ -Fe ₂ O ₃ -P	89.2	10.7	0.2	-
Ce-Fe	40.3	5.9	0.1	9.508
Ce@Ce-Fe	26.6	6.9	0.1	8.984
Ce@CeO ₂ -Fe ₂ O ₃	81.2	10.5	0.2	9.096

P represented precursors.

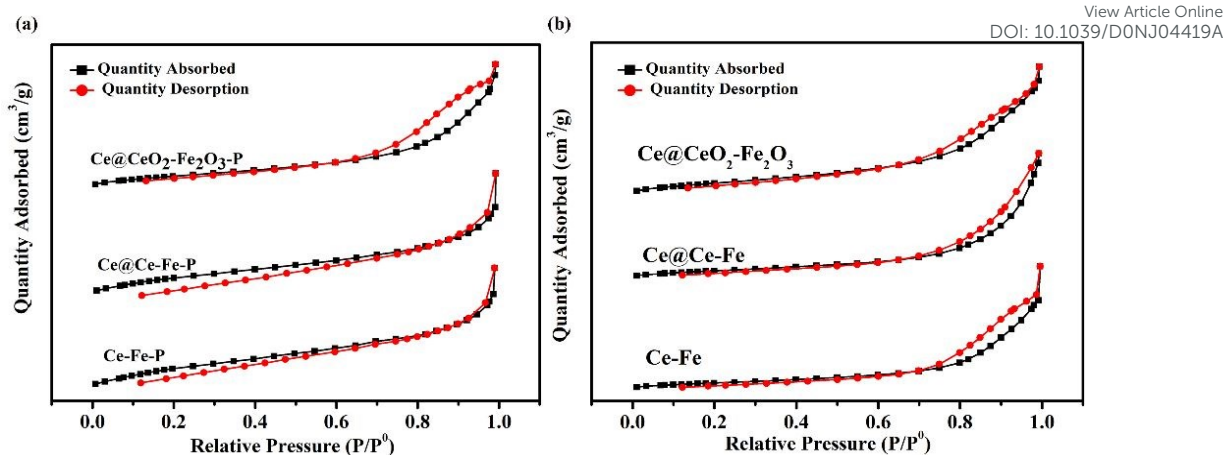


Fig. 4 N_2 adsorbed-desorption isotherms of precursors (a) and catalysts (b).

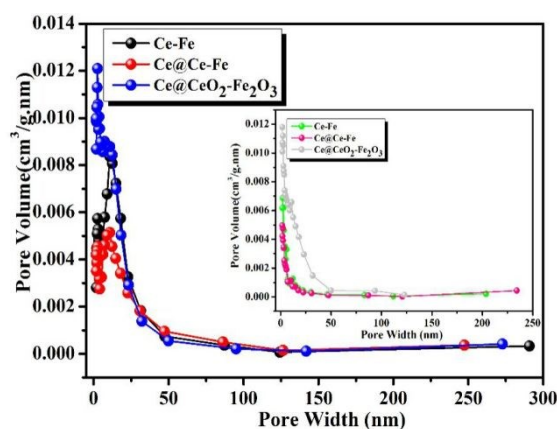


Fig. 5 Pore size distribution curves of catalysts. (Inner picture was a comparison about precursors)

3.3 Catalytic performance

The catalytic activity of these related Ce-Fe catalyst is shown in Fig. 6a. According to Fig. 6a, the conversion of Ce-Fe catalyst could reach 80 % at 300 °C and the conversion rate above 80 % could be kept up to 450 °C. Meanwhile, it was clear that the operating temperature window was relatively wide. Based on Ce-Fe catalyst, the amount of PVP was adjusted in the synthesis process, the concentration of metal salt Ce as well as the molar ratio between Ce and Fe to obtain catalyst Ce-Fe-PVP, Ce-Fe-C and Ce-Fe-M catalysts, respectively. For Ce-Fe-C catalyst, the NO conversion could reach 80 % at 260 °C, and arrive at the maximum at 320 °C,

which could reach 90 %. However, the operating temperature window was narrow, only changing from 260 °C to 360 °C. Specially, for the Ce-Fe-PVP and Ce-Fe-M catalysts, changing the amount of PVP in the Ce-Fe catalyst and the molar ratio between Ce and Fe would reduce the NO conversion as well as decrease the operating temperature window. Therefore, according to above summary, the synthesis condition of Ce-Fe catalyst was optimal. After exploring the synthesis conditions of Ce-Fe catalyst, the method of CeO₂ anchoring catalyst was adopted to promote the catalytic activity and board the temperature window. As shown in Fig. 6b, CeO₂ was anchored on the Ce-Fe catalyst precursor and the calcined CeO₂-Fe₂O₃ catalyst oxide to obtain Ce@Ce-Fe and Ce@CeO₂-Fe₂O₃ catalysts, respectively. In addition, three catalysts were tested at a temperature of 120 °C to 500 °C. For Ce@Ce-Fe catalyst, it had a higher NO conversion and a wider operating temperature window than the other two catalysts in the NH₃-SCR reaction. Specifically, the conversion rate of NO exceeded 80 % in the temperature range of 295 °C to 480 °C. In contrast, when the conversion rate of NO exceeded 80 %, the working temperature window of Ce-Fe and Ce@CeO₂-Fe₂O₃ catalysts would become narrower. At the same time, the Ce@Ce-Fe catalyst exhibited the best catalytic activity. When the temperature was 320 °C, the NO conversion near arrived at 92 %. However, for Ce@CeO₂-Fe₂O₃ catalyst, when the temperature was 260 °C, the conversion rate of NO reached 80 %. Although the low-temperature activity was excellent, the operating temperature window became very narrow. In detail, when the temperature was higher than 280 °C, the conversion rate of NO was less than 80 %. Therefore, among these three catalysts, the

1
2
3
4
5
6
7
8
9
10
11
12
13
14
15
16
17
18
19
20
21
22
23
24
25
26
27
28
29
30
31
32
33
34
35
36
37
38
39
40
41
42
43
44
45
46
47
48
49
50
51
52
53
54
55
56
57
58
59
60

Ce@CeO₂-Fe₂O₃ catalyst had the worst catalytic activity and the narrowest operating temperature window. Furthermore, Fig. S2 illustrates the N₂ selectivity and NH₃ conversion of the catalysts. As shown in Fig. S2, the N₂ selectivity almost kept slight decline during the whole test, indicating that all of the catalysts showed good N₂ selectivity for NH₃-SCR of NO. In terms of NH₃ conversion, when temperature was below 200°C for three catalysts, the NH₃ oxidation was very low and maintained a steady state. However, the temperature further increased to 240 °C, which led to a significantly higher conversion of NH₃ over Ce@CeO₂-Fe₂O₃. Meanwhile, a similar result was observed over Ce-Fe and Ce@CeO₂-Fe₂O₃ catalysts in inner picture of Fig.S2, which could be demonstrated that NH₃ was mainly oxidized to NO at high temperature. Furthermore, by combining the NO conversion results in the NH₃-SCR procedure with NH₃ oxidation, the decline of catalytic activity at high temperature was caused by the obvious increasing of oxidation of NH₃ with different catalysts. In summary, Ce@Ce-Fe catalyst had the best catalytic activity, board operating temperature window, and higher N₂ selectivity. Hence, it could be proved that Ce anchored Ce-Fe catalyst precursor was the best experimental modification scheme.

Schematic S1 explains the fabrication of catalysts in supplementary information.

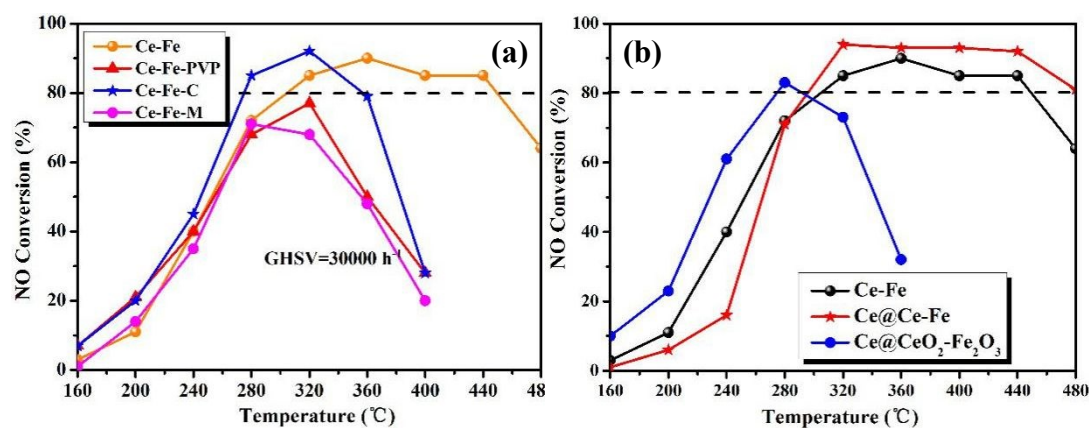


Fig. 6 NO conversion of different reaction temperature. Reaction conditions: [NO] =

[NH₃] = 500 ppm, [O₂] = 5 vol. %, balance N₂ and GHSV = 30,000 h⁻¹.

As we all know, air pollutants contained a part of water, so the resistance of water for catalysts was very significant in industry. As could be observed from Fig. 7a, the NO conversion of three catalysts did not change significantly during the whole resistance test of entire water. It was worth noting that the Ce-Fe catalyst could slowly recover its NO conversion after H₂O was turned off for two hours. For the Ce@CeO₂-Fe₂O₃ catalyst, the NO conversion fluctuated only slightly during the entire process, and there was no obvious change. And two hours after stopping the water flow, the conversion of NO could slowly recover to fresh condition. In addition, Ce@Ce-Fe catalyst had almost negligible effect on NO conversion during the resistance test of entire water, which indicated that Ce@Ce-Fe catalyst had good resistance of H₂O.

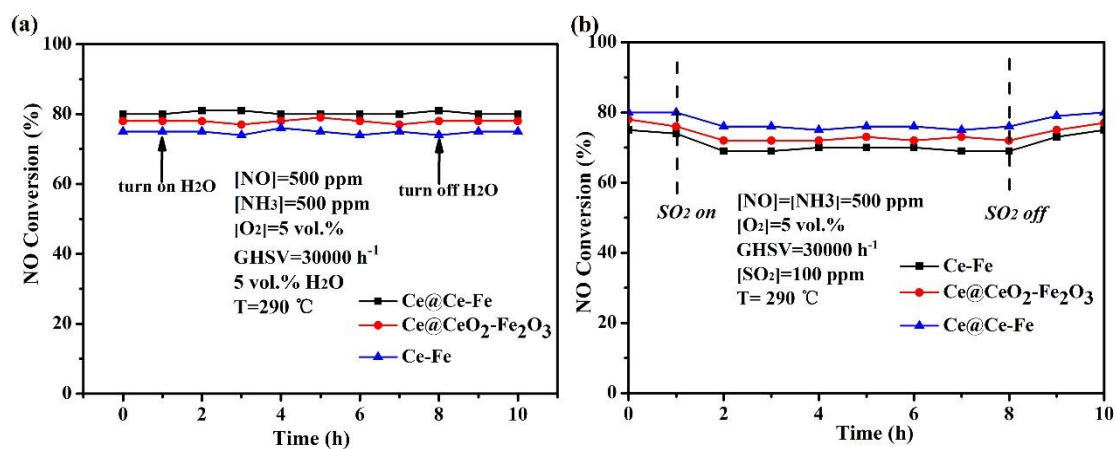


Fig. 7 NO_x conversion under H₂O conditions (a) and SO₂ conditions (b).

Generally, the sulfur dioxide in the flue gas had a fatal effect on the conversion of NO in the NH₃-SCR reaction, so it was necessary to explore the resistance of SO₂ of catalyst. Among them, the test conditions of Ce-Fe, Ce@Ce-Fe and Ce@CeO₂-Fe₂O₃ catalysts were: 100 ppm SO₂, 290 °C, GHSV = 30000 h⁻¹. According to Fig. 7b, it could be observed that the NO conversion of the Ce-Fe catalyst decreased from 75 % to 68 % within two hours after the SO₂ was introduced. At the same time, the NO conversion of the Ce@Ce-Fe catalyst was reduced from 78 % to 72 % within two hours after the SO₂ was introduced. Compared with the other two catalysts, the Ce@Ce-Fe catalyst had good resistance of SO₂ performance during the whole test. Before introducing SO₂, the NO conversion of Ce@Ce-Fe catalyst at 290 °C was 81 %, indicating good catalytic activity. However, once SO₂ was introduced, the NO conversion would drop sharply to 74 %. At the same time, in the next 6 hours of the resistance of SO₂ test, the NO conversion always fluctuated in the range of 73 % to 75 %. It should be emphasized that during the last two hours of the resistance of SO₂ test, the conversion of NO hardly changed, which might be the equilibrium state in which the catalyst was deactivated by the resistance of SO₂ reaction. In addition, when we stopped passing SO₂, the conversion of Ce@Ce-Fe catalyst could gradually recover to 79 % in the next two hours, which indicated that the catalyst had undergone competitive absorption between SO₂ and NH₃, resulting in the temporary deactivation of the catalyst. However, a stability test of 24 h was performed to examine the tolerance of SO₂ for our best catalyst in Fig. S3a. Furthermore, after long test of 24 h, the catalytic activity would basically keep stable.

1
2
3
4 Compared with previous test, the catalytic activity would not recover at initial
5
6
7 standard. It might be concluded that the surface of catalyst was formed cerium sulfate
8
9 species, which was hard to decompose on the surface of catalyst, resulting in the low
10
11 conversion of NO_x . According to Fig. S3b, when SO_2 and H_2O simultaneously added
12
13 into catalytic system, the NO conversion would be an obvious drop at once, indicating
14
15 that wet environment of SO_2 played a negative role in catalytic activity. Meanwhile,
16
17 after four hours of test, the deNO_x would keep stable until the end of test. Although,
18
19 after two hours of the end of test, the catalytic activity would be slowly rise, it would
20
21 not totally recover, indicating that the process was irreversible, which might be
22
23 explained that the surface of catalyst was formed cerium sulfate species, and
24
25 catalyst's active sites were blocked by those sulfates and the specific area was
26
27 decreased. Accordingly, the NH_4HSO_4 would decompose more easily after SO_2 and
28
29 H_2O were removed, which resulted in the recovery of the catalysts' activities to some
30
31 extent. Based on the above conclusions, it could be concluded that the Ce@Ce-Fe
32
33 catalyst had relatively satisfactory performance about the resistance of SO_2 in the
34
35 NH_3 -SCR reaction.
36
37
38
39
40
41
42
43
44
45
46
47
48
49
50
51
52
53
54
55
56
57
58
59
60

3.4 Catalytic reducibility

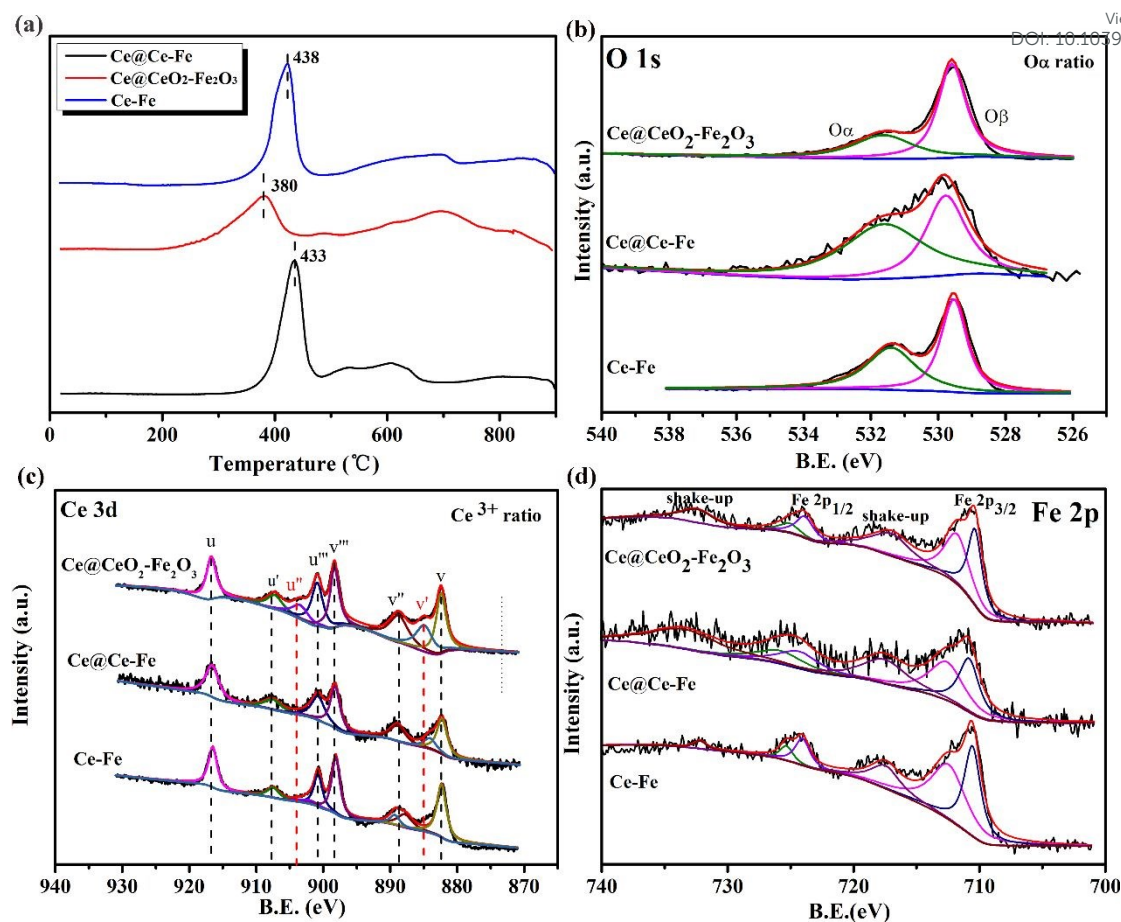


Fig. 8 H₂-TPR profiles of different catalysts (a), XPS spectra of O 1s (b), Ce 3d (c), Fe 2p (d).

It was generally believed that the redox activity of the catalyst was critical to the catalytic cycle in the NH₃-SCR process. H₂-TPR was an effective technique for evaluating the reducibility of cerium and iron species on these three catalysts. According to Fig. 8a, the three catalysts showed peaks at 440 and 650 °C, indicating that the catalysts gradually reduced Fe₂O₃ to Fe metal [33]. The TPR curve of the Fe-Ce sample attributed the low-temperature peak (about 400 °C) to the first-step reduction of Fe³⁺ inside the Ce-Fe-O solid solution and the simultaneous reduction of Ce⁴⁺ on the solid solution surface [34]. Meanwhile, the further reduction process (reduction peaks at about 600 and 800 °C) was considered to be related to the

intermediate reduction step of iron oxide and the overall reduction of Ce^{4+} [35]. In addition, for $\text{Ce@CeO}_2\text{-Fe}_2\text{O}_3$ catalyst, because its reduction temperature was the lowest, so its catalytic activity of low temperature was the best. This conclusion was consistent with the conversion of NO, as shown in Fig. 6b. Moreover, for Ce-Fe catalyst and Ce@Ce-Fe catalyst, the peak intensity of Ce@Ce-Fe was stronger, and the peak appearing at 600 °C was more obvious, indicating that there was mutual synergy between Ce and Fe, which could be explained that Ce@Ce-Fe catalyst had better catalytic performance and wider operating temperature window than Ce-Fe catalyst [36].

Table 2 XPS results for surface atomic concentration (%)

Sample	Ce	Fe	O	$O_\alpha / (O_\alpha + O_\beta)$	$\text{Ce}^{3+} / (\text{Ce}^{3+} + \text{Ce}^{4+})$	Fe/Ce	$\text{Fe}^{3+} / \text{Fe}^{2+}$
Ce-Fe	13.35	11.91	74.65	46.33	7.81	0.89	1.49
Ce@Ce-Fe	14.90	11.94	73.11	58.33	19.47	0.80	2.49
$\text{Ce@CeO}_2\text{-Fe}_2\text{O}_3$	17.97	11.00	71.02	35.20	13.28	0.61	1.83
Ce@Ce-Fe-U	4.32	4.32	78.87	12.48	61.90	18.27	1.83

U represented the tolerance of H_2O and SO_2 .

XPS analysis was performed on Ce-Fe, Ce@Ce-Fe and $\text{Ce@CeO}_2\text{-Fe}_2\text{O}_3$ catalysts to clarify the surface atomic concentration and valence state of all elements in these three catalysts. The surface atomic concentrations of Fe, Ce and O are measured and summarized in Table 2. The corresponding XPS spectra of Fe, Ce and O are shown in Fig. 8b-d. As shown in Fig. 8b, the XPS spectrum of O 1s was fitted

to two peaks, one of which had a lower binding energy (529.5 eV) corresponding to lattice oxygen (expressed as O_{β}) and the other was located at a higher binding energy (531.7 eV) corresponded to chemisorbed oxygen (denoted as O_{α}) [37]. Chemically adsorbed oxygen (O_{α}) was a better active oxygen because it had a higher mobility and acted a significant role in the SCR reaction. It could be observed from Table 2 that the percentage of O_{α} species on the surface of Ce@Ce-Fe (58.33 %) was much higher than that of Ce-Fe (46.33 %), which was attributed to the structural difference of the Ce anchoring catalyst. In addition, the percentage of O_{α} species on the surface of Ce@Ce-Fe was also higher than the percentage of Ce@CeO₂-Fe₂O₃ (35.20 %). Hence, Ce@Ce-Fe had the best catalytic activity among three catalysts. In summary, chemically adsorbed oxygen (O_{α}) played a key role in the NH₃-SCR reaction.

Fig. 8c shows Ce 3d XPS spectra of three catalysts. The XPS spectrum of Ce 3d usually was consisted of eight peaks, namely v (882.4 eV), v' (885.9 eV), v'' (889.8 eV), v''' (898.7 eV), u (901.3 eV), u' (904.5 eV), u'' (907.8 eV) and u''' (917.1 eV). Among them, the peaks of v, v'', v''', u, u'' and u''' corresponded to the initial electronic state of 3d104f0 of Ce⁴⁺ species, while the peaks of v' and u' were due to the initial electronic state of 3d104f1 corresponding to Ce³⁺ species [38]. Generally, a higher Ce³⁺ ratio indicated that there were more oxygen vacancies on the surface of the catalyst, which might facilitate the conversion of active oxygen species, increase the oxidation of NO to NO₂, and promote the adsorption and activation of reactants. Table 2 summarizes the surface concentration of Ce³⁺ on the surface of Ce-Fe, Ce@Ce-Fe and Ce@CeO₂-Fe₂O₃. It could be observed that the percentage of Ce³⁺ on

1
2
3
4 the surface of Ce@Ce-Fe (19.47 %) was much higher than the percentage of Ce-Fe
5
6 (7.81 %). After Ce was anchored on the Ce-Fe catalyst, the Ce³⁺ surface concentration
7
8 was higher than the Ce-Fe surface concentration, indicating that Ce successfully
9
10 anchored the surface of Ce-Fe catalyst and the catalytic activity got improved after Ce
11
12 anchoring. At the same time, oxygen vacancies on the catalyst could be generated by
13
14 the electron conversion between Ce³⁺ and Ce⁴⁺, and higher Ce³⁺ concentration could
15
16 form more oxygen vacancies, indicating that the oxygen vacancy of Ce@Ce-Fe was
17
18 much more than that of Ce-Fe.
19
20
21
22
23
24
25
26
27
28
29
30
31
32
33
34
35
36
37
38
39
40
41
42
43
44
45
46
47
48
49
50
51
52
53
54
55
56
57
58
59
60

As displayed in the high-resolution XPS spectrum of Fe 2p (Fig. 8d), the peaks located at 711.4 and 725.2 eV, along with two shake-up satellite peaks at 717.9 and 732.5 eV, could be attributed to Fe³⁺, and another two peaks centered at 710.5 and 723.8 eV could be ascribed to Fe²⁺ [39]. Apparently, the Fe element was present in the chemical state of Fe³⁺ and Fe²⁺. For the Ce@Ce-Fe catalyst, the peak shifted towards a higher binding energy than Ce-Fe, which indicated that Ce was anchored on the Ce-Fe catalyst and the interaction between Ce and Fe occurred on the surface of catalysts [31]. Meanwhile, Ce@Ce-Fe catalyst had highest the ratio of Fe³⁺/Fe²⁺ (2.49) among three catalysts. According to previous reports, the available Fe³⁺ could participate in the reversible redox cycle, which was beneficial to the SCR catalytic activity. In addition, a more appropriate Fe³⁺ ratio was conducive to the reduction of NO, thereby improving the catalytic activity. In summary, Ce@Ce-Fe catalyst with higher surface atomic concentration of Fe (11.94 %) and Fe³⁺/Fe²⁺ (2.49) had better NH₃-SCR performance.

3.5 Surface acidities

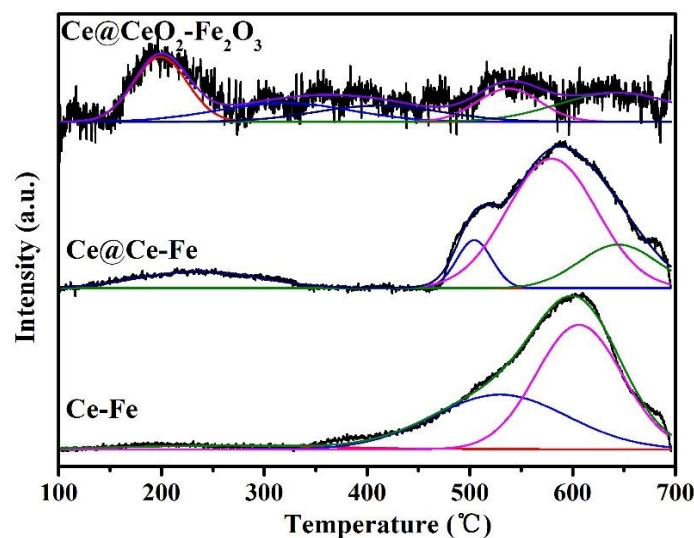


Fig. 9 NH₃-TPD profiles of different catalysts.

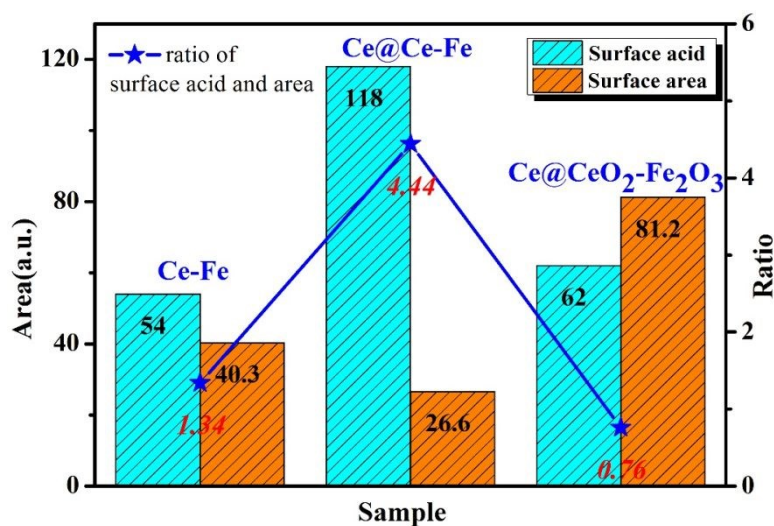


Fig. 10 The relationship of surface acid and surface area among three catalysts.

Surface acidities were beneficial to the SCR catalysts because of efficient absorption of NH₃. Therefore, NH₃-TPD was evaluated to investigate the effect of surface acidities on the performance of catalysts for NH₃-SCR reaction. In addition, Ce-Fe, Ce@Ce-Fe and Ce@CeO₂-Fe₂O₃ catalyst profiles are presented in Fig. 9, which could be divided into four or five peaks ranged from 100 °C to 700 °C.

Notably, for Ce@Ce-Fe catalyst, the peaks at 240 °C was assigned to middle strong acid, which was considered to be significant for NH₃-SCR reaction. Meanwhile, for Ce@CeO₂-Fe₂O₃ catalyst, the peak at 200°C was ascribed to weak acid. As a comparison, for Ce-Fe catalyst, it only appeared strong acid, owing weak surfaced acidities. Notably, the amount of ammonia desorbed had been determined and normalized with respect to the specific surface area, which are shown in Table 3 and Fig. 10. On the one hand, it was clear that Ce@Ce-Fe had the biggest surface acid and average acid by calculation from surface area, indicating that surface acid sites acted a significant role in the process of NH₃-SCR reaction. On the other hand, the NH₃-TPD results demonstrate that the Ce@Ce-Fe catalyst present not only the larger acid amount but also stronger acid strength, which could facilitate the chemisorption and activation of NH₃, resulting in the better performance in the NH₃-SCR of NO. Therefore, it was worth noting that the amount of surface acidities with weak and middle strong acid obviously increased after the anchoring of Ce on Ce-Fe catalyst. In summary, abundant surface acidities mainly including weak and middle strong acid sites might be essential for a better catalytic activity in NH₃-SCR system.

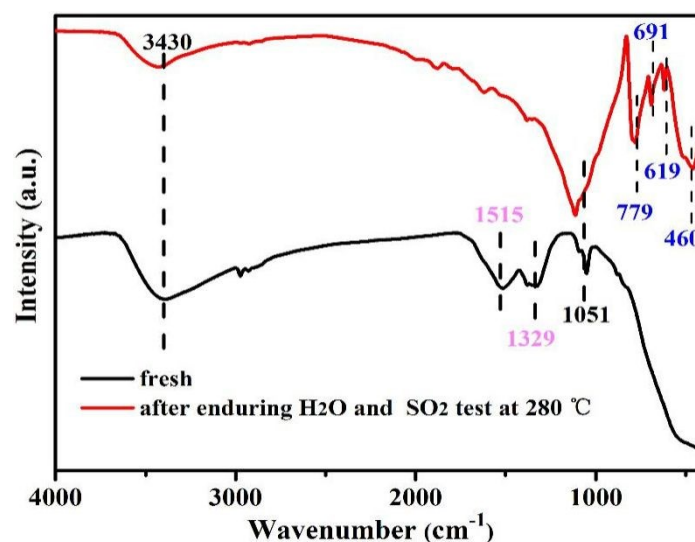
Table 3 The amount of surface acid sites.

sample	Weak acid		Middle strong acid		Sum area (a.u.)
	T ^a (°C)	Area (a.u.)	T ^a (°C)	Area (a.u.)	
Ce-Fe	-	-	266	54	54
Ce@Ce-Fe	-	-	237	118	118
Ce@CeO ₂ -Fe ₂ O ₃	200	36	320	26	62
Ce@Ce-Fe-U	-	-	285	21	21

^a The peak at temperature (°C), U represented the tolerance of H₂O and SO₂. View Article Online
DOI: 10.1039/D0NJ04419A

3.6 The physical and chemical properties of catalysts after enduring SO₂ test

The FTIR test is conducted to explore the effect of H₂O and SO₂ on catalytic performance in Fig. 10. Firstly, the peak appearing at 3430 cm⁻¹ might be caused by the surface hydroxyl material (O-H), and the vibration of N-H might appear at 3184 cm⁻¹ through the vibration area [40]. In addition, the band vibration of NH₄⁺ might occur at 1725 cm⁻¹ belonging to the Bronsted acid site [41]. Meanwhile, the peak between 1000 and 1300 cm⁻¹ corresponded to the tensile vibration of the C-O bond, which might be likely related to the presence of carbonates. Furthermore, the bands appearing at 1515 cm⁻¹ and 1329 cm⁻¹ were attributed to the Lewis acid site and the coordination NH₃ on the Lewis acid site, respectively [42]. Meanwhile, the symmetric bending vibration of NH₄⁺ species might appear at 2957 cm⁻¹, which indicated that the adsorption of NH₃ was formed on the acidic sites of the surface [43]. After the reaction, a small band at 619 cm⁻¹ could be assigned to the new Fe-O phase formed on the surface of the Fe-Ce catalyst [44]. After the reaction of H₂O and SO₂, a new peak at 1122 cm⁻¹, which corresponds to the characteristic band of SO₄²⁻ [45]. Therefore, the introduction of SO₂ led to the formation of by-products such as (NH₄)₂SO₃ and NH₄HSO₄. Because the sulfate formed occupied the active site on the surface of the Ce@Ce-Fe catalyst, the NO conversion might decrease, which was mainly related to the deposition of ammonium sulfate or ammonium sulfite.



View Article Online
DOI: 10.1039/D0NJ04419A

Fig. 11 FTIR spectra of catalysts: fresh catalysts and after SO₂ test.

After H₂O and SO₂ enduring test, the chemical state of element is also explored to compare Ce@Ce-Fe and Ce@Ce-Fe-U catalyst by XPS methods in Table 2 and Fig. 12. Apparently, compared with fresh catalyst, O_a ratio of Ce@Ce-Fe catalyst decreased after enduring SO₂ test at 290 °C, which might be an important reason for the decline of catalytic activity. Another reason was that SO₂ could react with H₂O and NH₃ to form NH₄HSO₄, which could block the active sites. Meanwhile, on the one hand, the surface atomic ratio of Ce³⁺/ (Ce³⁺ + Ce⁴⁺) was slightly lower than fresh catalyst, illustrating that the oxide of Ce³⁺ species was restrained. Furthermore, SO₂ with Ce³⁺ could easily form cerium sulfate species, which was hard to decompose on the surface of catalyst, which might result in the low conversion of NO_x. On the other hand, the influence of SO₂ on acidic properties is explored in Table 3 and Fig. S4. Obviously, the effective acid amount would be declined, indicating that SO₂ exposure led to significant changes on the acidic properties. According to above analysis, the declination of O_a ratio, the formation of NH₄HSO₄ and cerium sulfate

species might lead to low catalytic activity.

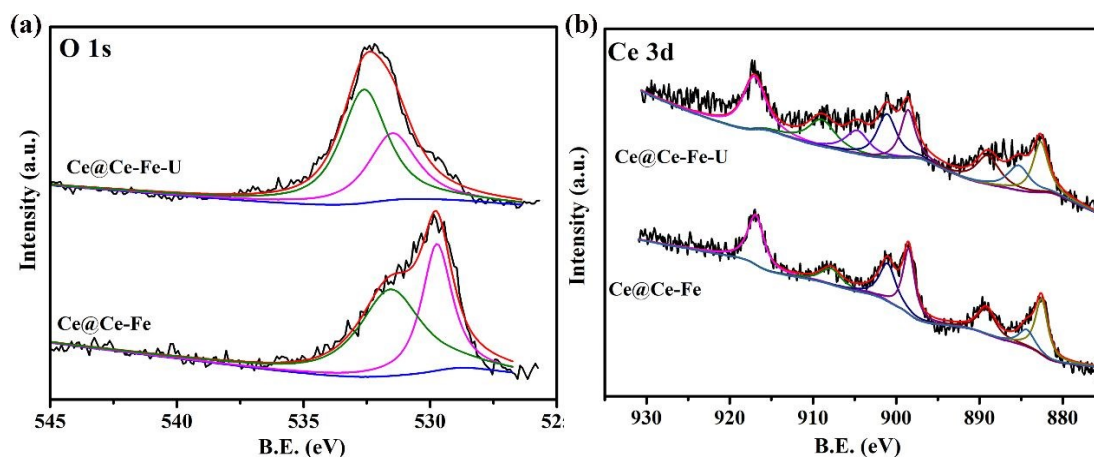


Fig.12 XPS spectra of O 1s and Ce 3d after H₂O as well as SO₂ test.

4 Conclusions

In summary, we had successfully fabricated Ce@Ce-Fe Prussian blue analogues with unique morphology and structure as good performance deNO_x catalysts via anchoring of Ce on the surface of Ce-Fe, which were derived from Ce-Fe precursors synthesized via a simple co-precipitation method. The double-cone structure Ce@Ce-Fe catalyst displayed enhanced catalytic activity, wider working temperature window and improved tolerance of H₂O and SO₂. It has been demonstrated that the characteristic of unique double-cone structure, the uniform distribution of active sites, as well as the strong redox performance were attributed to the enhanced catalytic performance of Ce@Ce-Fe catalyst in NH₃-SCR. The feature of unique morphology and mesoporous structures supplies a larger surface area and more active sites to adsorb and activate reagents, resulting in the higher catalytic activity. Moreover, excellent redox performance and high content of Fe atoms resulted in high catalytic cycle stability and improved SO₂ tolerance. Meanwhile, acidic properties also acted a

significant role in catalytic performance. Based on our work, this study may provide an approach and idea for development of mixed metal oxides with unique structure and modification of NO_x activity for NH₃-SCR reaction.

Acknowledgement

This work was supported by the National Natural Science Foundation of China (51808529), the Major Project of Inner Mongolia Science and Technology (2019ZD018), the DNL Cooperation Found, CAS (DNL201906).

References

- [1] D.A.P.a. Panagiotis G. Smirniotis, and Balu S. Uphade, *Angew. Chem. Int. Ed.*, 2001, 40, 2479-2482.
- [2] Colin J, Jim H, Gordan M., *Nature*, 1992, 355 (2):69-71.
- [3] Barbara J. Finlayson P. James N, *Science*, 276 (16): 1045-1052
- [4] L. Kang, L. Han, J. He, H. Li, T. Yan, G. Chen, J. Zhang, L. Shi, D. Zhang, *Environ. Sci. Technol.*, 53 (2019) 938-945.
- [5] L. Han, M. Gao, J.Y. Hasegawa, S. Li, Y. Shen, H. Li, L. Shi, D. Zhang, *Environ. Sci. Technol.*, 53 (2019) 6462-6473.
- [6] C.H. Kim, G. Qi, K. Dahlberg, W. Li, *Science*, 327 (2010) 1624-1627.
- [7] L. Han, M. Gao, C. Feng, L. Shi, D. Zhang, *Environ. Sci. Technol.*, 53 (2019) 5946-5956.
- [8] A.M. Beale, F. Gao, I. Lezcano-Gonzalez, C.H. Peden, J. Szanyi, *Chem. Soc. Rev.*, 44 (2015) 7371-7405.
- [9] S. Brandenberger, O. Kröcher, A. Tissler, R. Althoff, *Catal. Rev.*, 50 (2008)

492-531.

[10] J. Xu, H. Yu, C. Zhang, F. Guo, J. Xie, *New J. Chem.*, 43 (2019) 3996-4007.

[11] L. Chen, Z. Si, X. Wu, D. Weng, R. Ran, J. Yu, *J. Rare Earth*, 32 (2014) 907-917.

[12] W. Shan, F. Liu, Y. Yu, H. He, *Chinese J. Catal.*, 35 (2014) 1251-1259.

[13] C. Tang, H. Zhang, L. Dong, *Catal. Sci. Technol.*, 6 (2016) 1248-1264.

[14] H. Liu, Z. Fan, C. Sun, S. Yu, S. Feng, W. Chen, D. Chen, C. Tang, F. Gao, L. Dong, *Appl. Catal. B: Environ.*, 244 (2019) 671-683.

[15] X. Li, J. Li, Y. Peng, H. Chang, T. Zhang, S. Zhao, W. Si, J. Hao, *Appl. Catal. B: Environ.*, 184 (2016) 246-257.

[16] J. Liu, X. Li, Q. Zhao, J. Ke, H. Xiao, X. Lv, S. Liu, M. Tadé, S. Wang, *Appl. Catal. B: Environ.*, 200 (2017) 297-308.

[17] Y. Peng, K. Li, J. Li, *Appl. Catal. B: Environ.*, 140-141 (2013) 483-492.

[18] Y. Peng, C. Liu, X. Zhang, J. Li, *Appl. Catal. B: Environ.*, 140-141 (2013) 276-282.

[19] R. Qu, X. Gao, K. Cen, J. Li, *Appl. Catal. B: Environ.*, 142-143 (2013) 290-297.

[20] N. Husnain, E. Wang, K. Li, M.T. Anwar, A. Mehmood, M. Gul, D. Li, J. Mao, *Rev. Chem. Eng.*, 35 (2019) 239-264.

[21] F. Liu, Y. Yu, H. He, *Chem. Commun.*, 50 (2014) 8445-8463.

[22] W. Shan, H. Song, *Catal. Sci. Technol.*, 5 (2015) 4280-4288.

[23] H. Zou, C. Yuan, H. Zou, T. Cheang, S. Zhao, L. Wang, A. Xu, *Catal. Sci. Technol.*, 7 (2017) 1549-1555.

- 1
2
3
4 [24] L. Liu, J. Shi, R. Wang, H. Cao, Z. Liu, *J. Alloy Compd.*, 725 (2017) 544-556. View Article Online
DOI: 10.1039/D0NJ04419A
- 5
6
7 [25] L. Hu, P. Zhang, Q.W. Chen, N. Yan, J.Y. Mei, *Dalton Trans.*, 40 (2011)
8
9 5557-5562.
- 10
11
12 [26] L. Hu, J.Y. Mei, Q.W. Chen, P. Zhang, N. Yan, *Nanoscale*, 3 (2011) 4270-4274.
- 13
14 [27] L. Yan, Y. Liu, K. Zha, H. Li, L. Shi, D. Zhang, *ACS Appl. Mater. Interf.*, 9
15
16 (2017) 2581-2593.
- 17
18
19 [28] L. Zhang, L. Shi, L. Huang, J. Zhang, R. Gao, D. Zhang, *ACS Catal.*, 4 (2014)
20
21 1753-1763.
- 22
23 [29] J. Han, J. Meeprasert, P. Maitarad, S. Nammuangruk, L. Shi, D. Zhang, *J. Phys.*
24
25 *Chem. C*, 120 (2016) 1523-1533.
- 26
27
28 [30] S. Yang, Y. Guo, H. Chang, L. Ma, Y. Peng, Z. Qu, N. Yan, C. Wang, J. Li,
29
30 *Appl. Catal. B: Environ.*, 136-137 (2013) 19-28.
- 31
32 [31] X. Zhang, J. Wang, Z. Song, H. Zhao, Y. Xing, M. Zhao, J. Zhao, Z.a. Ma, P.
33
34 Zhang, N. Tsubaki, *Mol. Catal.*, 463 (2019) 1-7.
- 35
36
37 [32] Z. Chen, F. Wang, H. Li, Q. Yang, L. Wang, X. Li, *Ind. Eng. Chem. Res.*, 51
38
39 (2011) 202-212.
- 40
41
42 [33] Z. Ma, D. Weng, X. Wu, Z. Si, *J. Environ. Sci.*, 24 (2012) 1305-1316.
- 43
44
45 [34] K. Zhou, X. Wang, X. Sun, Q. Peng, Y. Li, *J. Catal.*, 229 (2005) 206-212.
- 46
47
48 [35] C. Bigey, L. Hilaire, G. Maire, *J. Catal.*, 198 (2001) 208-222.
- 49
50
51 [36] J. Engweiler, J. Harf, A. Baiker, *J. Catal.*, 159 (1996) 259-269.
- 52
53
54 [37] J.-C. Dupin, D. Gonbeau, P. Vinatier, A. Levasseur, *Phys. Chem. Chem. Phys.*, 2
55
56 (2000) 1319-1324.
57
58
59
60

- [38] G. Zhang, W. Han, F. Dong, L. Zong, G. Lu, Z. Tang, RSC Adv., 6 (2016) 76556-76567.
- [39] F. Liu, W. Shan, Z. Lian, J. Liu, H. He, Appl. Catal. B: Environ., 230 (2018) 165-176.
- [40] Y. He, M.E. Ford, M. Zhu, Q. Liu, Z. Wu, I.E. Wachs, Appl. Catal. B: Environ., 188 (2016) 123-133.
- [41] M.A. Centeno, I. Carrizosa, J.A. Odriozola, Appl. Catal. B: Environ., 29 (2001) 307-314.
- [42] K. Wijayanti, K. Leistner, S. Chand, A. Kumar, K. Kamasamudram, N.W. Currier, A. Yezerets, L. Olsson, Catal. Sci. Technol., 6 (2016) 2565-2579.
- [43] A.S. Mamede, E. Payen, P. Grange, G. Poncelet, A. Ion, M. Alifanti, V.I. Pârvulescu, J. Catal., 223 (2004) 1-12.
- [44] X. Huang, G. Zhang, F. Dong, Z. Tang, J. Ind. Eng. Chem., 69 (2018) 66-76.
- [45] G. Zhang, Z. Yan, Commun. Nonlinear Sci., 62 (2018) 117-133.